3. Funato M, Fukao T, Sasai H, Hori T, Terazawa D, Kubota K, Ozeki M, Orii K, Kaneko H, Kondo N. Successful treatment of pediatric immune thrombocytopenic purpura associated with ulcerative colitis. ***Pediatr Int***. 2011 Oct; 53(5): 771-3.

4. Funato M, Kaneko H, Kubota K, Ozeki M, Kanda K, Orii K, Kato Z, Fukao T, Kondo N. Pediatric acute lymphoblastic leukemia mimicking Henoch-Schönlein purpura. ***Pediatr Int***. 2011 Oct; 53(5): 766-8.

5. Funato M, Kaneko H, Ohkusu K, Sasai H, Kubota K, Ohnishi H, Kato Z, Fukao T, Kondo N. Refractory chronic pleurisy caused by Helicobacter equorum-like bacterium in a patient with X-linked agammaglobulinemia. ***J Clin Microbiol***. 2011 Sep; 49(9): 3432-5.

6. Kaneko H, Fukao T, Kasahara K, Yamada T, Kondo N. Augmented cell death with Bloom syndrome helicase deficiency. ***Mol Med Report***. 2011 4(4): 607-9.

7. An Y, Ohnishi H, Matsui E, Funato M, Kato Z, Teramoto T, Kaneko H, Kimura T, Kubota K, Kasahara K, Kondo N. Genetic variations in MyD88 adaptor-like are associated with atopic dermatitis. ***Int J Mol Med***. 2011 Jun; 27(6): 795-801.

8. Morita H, Kaneko H, Ohnishi H, Kato Z, Kondo N. Antigen-specific immune response to endotoxin-free recombinant P34. ***Allergy***. 2011 Jul; 66(7): 985-6.

9. Morita H, Kaneko H, Ohnishi H, Kato Z, Kondo N. Antigen-specific immune response to endotoxin-free recombinant P34. ***Allergy***. 2011 Jul; 66(7): 985-6.

10. Kaneko H, Fukao T, Kasahara K, Yamada Y, Kondo N Augmented cell death with human and mouse Bloom syndrome helicase deficiency. ***Mol Med Rep***. 2011 Jul-Aug; 4(4): 607-9.

11. Kaneko H, Teramoto T, Kondo M, Morita H, Ohnishi H, Orii K, Matsui E, Kondo N. Efficacy of the slow dose-up method for specific oral tolerance induction for children in cow's milk allergy: Comparison with previous reported protocols. ***Journal of Investigational Allergology and Clinical Immunology***. 2010. 20: 538-9.

12. Matsui E, Shinoda S, Fukutomi O, Kaneko H, Fukao T, Kondo N. Relationship between the benefits of suplatast tosilate, a Th2 cytokine inhibitor, and gene polymorphisms in children with bronchial asthma. ***Experimental and therapeutic medicine***. 2010. 1: 977-82.

13. Kondo N, Matsui E, Nishimura A, Kaneko H. Pharmacogenetics of asthma in children. ***Allergy Asthma Immunol Res***. 2010. 2: 14-9.

14. Ozeki M, Funato M, Teramoto T, Ohe N, Asano T, Kaneko H, Fukao T, Kondo N.Reversible cerebrospinal fluid edema and porencephalic cyst, a rare complication of ventricular catheter.***J Clin Neurosci***. 2010. 17: 658-61.

15. Ozeki M, Kunishima S, Kasahara K, Funato M, Teramoto T, Kaneko H, Fukao T, Kondo N. A family having type 2B von Willebrand disease with an R1306W mutation: Severe thrombocytopenia leads to the normalization of high molecular weight multimers. ***Thromb Res***. 2010. 125: e17-22.

2. 学会発表

1. Kaneko H, Ohnishi H, Morita H, Yamamoto T, Kubota K, Teramoto T, Kato Z, Matsui E, Kato H, Nakano T, Kondo N. Development of enzymatically digested peptides for immunomodulation therapy in patients with cow's milk allergy. 16th Asia Pacific Association of Pediatric Allergy, Respiratory and Immunology. Fukuoka, Japan. Oct 28～30, 2011.

2. Kaneko H, Ohnishi H, Funato M, Kondo N. Pathogenesis and clinical feature of primary antibody deficiencies. The 7th Congress of Asian Society for Pediatric

Research. Denver, Colorado, USA. Apr. 30～May. 3, 2011.

3. Kaneko H, Suzuki H, Kondo N. : Workshop Various expression patterns of alpha1 and alpha2 genes in IgA deficiency. : Primary immunodeficiency. 4th Intenantional Congress of Immunology. Kobe, Japan. Aug. 2010.

4. 金子英雄, 深尾敏幸, 谷内江昭宏, 清河信敬, 滝田順子, 内田靖, 近藤直実. Bloom 症候群の実態調査と診断指針の策定の試み　第 4 回日本免疫不全症研究会. 2011 年 1 月 22 日 福岡

5. 金子英雄, 大西秀典, 森田秀行, 川本美奈子, 久保田一生, 寺本貴英, 加藤善一郎, 松井永子, 加藤晴彦, 中埜拓, 近藤直実: シンポジウム　食物アレルギーの発症・増悪を修飾する因子ー「食べて治す食品(2005 岐阜)」開発への展開ー: アレルギー疾患の経過を修飾する因子　第 47 回日本小児アレルギー学会. 2010 年 12 月 横浜

6. Kaneko H, Morita H, Ohnishi H, Kato Z, Matsui E, Kondo N. Expression and purification of recombinant soybean protein P34 and its clinical application. The 8th Asia Pacific Congress of Allergy, Asthma and Clinical Immunology. Singapore. Nov. 2010.

7. 金子英雄, 松井永子, 大西秀典, 安陽, 加藤善一郎, 松井猛彦, 岩田力, 勝沼俊雄, 南部光彦, 岡田賢司, 近藤直実: シンポジウム 小児喘息の新型インフルエンザによる肺炎合併症の発症機序: 新型インフルエンザと喘息について多面的に考える第 60 回日本アレルギー学会　秋季学術集会. 2010 年 11 月 東京

H. 知的財産権の出願・登録状況
(予定を含む)

1. 特許取得
なし

2. 実用新案登録
なし

3. その他
なし

Ⅳ．　研究成果に関する刊行の一覧表

研究成果の刊行に関する一覧表

雑 誌

発表者氏名	論文タイトル名	発表誌名	巻号	ページ	出版年
Nakamura K, Du L, Tunuguntla R, Fike F, Cavalieri S, Morio T, Mizutani S, Brusco A, Gatti RA.	Functional characterization and targeted correction of ATM mutations identified in Japanese patients with ataxia-stelangiectasia.	Hum Mutat.	33(1)	198-208	2012
Hayashi M, et al.	Lesions of cortical GABAergic interneurons and acetylcholine neurons in xeroderma pigmentosum group A.	Brain Dev	34(4)	287-92	2012
Hayashi M, et al.	Brain vascular changes in Cockayne syndrome.	Neuropathology	32(2)	113-7	2012
Kaneko H, Fukao T, Kasahara K, Yamada T, Kondo N.	Augmented cell death with Bloom syndrome helicase deficiency.	Mol Med Report.	4(4)	607-9	2011
Atsumi Y, Fujimori H, Fukuda H, Inase A, Shinohe K, Yoshioka Y, Shikanai M, Ichijima Y, Unno J, Mizutani S, Tsuchiya N, Hippo Y, Nakagama H, Masutani M, Teraoka H, Yoshioka K.	Onset of quiescence following p53 mediated down-regulation of H2AX in normal cells.	PLoS One.	6(8)	e23432	2011
Sakasai R, Teraoka H, Takagi M, Tibbetts RS.	Transcription - dependent activation of ataxia telangiectasia-mutated prevents DNA-dependent protein kinase - mediated cell death in response to topoisomerase I poison.	J Biol Chem.	285 (20)	15201-8	2010
Oba D, Hayashi M, Minamitani M, Hamano S, Uchisaka N, Kikuchi A, Kishimoto H, Takagi M, Morio T, Mizutani S.	Autopsy study of cerebellar degeneration in siblings with ataxia-telangiectasia-like disorder.	Acta Neuropathol.	119 (4)	513-20	2010
Ichijima Y, Yoshioka K, Yoshioka Y, Shinohe K, Fujimori H, Unno J, Takagi M, Goto H, Inagaki M, Mizutani S, Teraoka H.	DNA lesions induced by replication stress trigger mitotic aberration and tetraploidy development.	PLoS One.	5(1)	e8821	2010 Jan 21.
Miyata R, Sasaki T, Hayashi M, et al.	Low dose of levodopa is effective for laryngeal dystonia in xeroderma pigmentosum group A.	Brain Dev	32(8)	685-7	2010

Ⅴ．別刷

RESEARCH ARTICLE

Human Mutation

OFFICIAL JOURNAL
HGVS
HUMAN GENOME VARIATION SOCIETY
www.hgvs.org

Functional Characterization and Targeted Correction of ATM Mutations Identified in Japanese Patients with Ataxia-Telangiectasia

Kotoka Nakamura,[1] Liutao Du,[1] Rashmi Tunuguntla,[1] Francesca Fike,[1] Simona Cavalieri,[2] Tomohiro Morio,[3] Shuki Mizutani,[3] Alfredo Brusco,[2] and Richard A. Gatti[1,4]*

[1]*Department of Pathology and Laboratory Medicine, UCLA School of Medicine, Los Angeles, California;* [2]*Department of Genetics, Biology and Biochemistry, University of Torino, Medical Genetics Unit, S. Giovanni Battista Hospital, Torino, Italy;* [3]*Department of Pediatrics and Developmental Biology, Tokyo Medical and Dental University Graduate School of Medicine, Tokyo, Japan;* [4]*Department of Human Genetics, UCLA School of Medicine, Los Angeles, California*

Communicated by Michel Goossens

Received 14 June 2011; accepted revised manuscript 15 September 2011.
Published online 17 October 2011 in Wiley Online Library (www.wiley.com/humanmutation).DOI: 10.1002/humu.21632

ABSTRACT: A recent challenge for investigators studying the progressive neurological disease ataxia-telangiectasia (A-T) is to identify mutations whose effects might be alleviated by mutation-targeted therapies. We studied *ATM* mutations in eight families of Japanese A-T patients (JPAT) and were able to identify all 16 mutations. The probands were compound heterozygotes in seven families, and one (JPAT2) was homozygous for a frameshift mutation. All mutations—four frameshift, two nonsense, four large genomic deletions, and six affecting splicing—were novel except for c.748C>T found in family JPAT6 and c.2639-384A>G found in family JPAT11/12. Using an established lymphoblastoid cell line (LCL) of patient JPAT11, ATM protein was restored to levels approaching wild type by exposure to an antisense morpholino oligonucleotide designed to correct a pseudoexon splicing mutation. In addition, in an LCL from patient JPAT8/9, a heterozygous carrier of a nonsense mutation, ATM levels could also be partially restored by exposure to readthrough compounds (RTCs): an aminoglycoside, G418, and a novel small molecule identified in our laboratory, RTC13. Taken together, our results suggest that screening and functional characterization of the various sorts of mutations affecting the *ATM* gene can lead to better identification of A-T patients who are most likely to benefit from rapidly developing mutation-targeted therapeutic technologies.
Hum Mutat 33:198–208, 2012. © 2011 Wiley Periodicals, Inc.

KEY WORDS: ataxia-telangiectasia; ATM; large genomic deletions; functional analysis of DNA variants; mutation-targeted therapy; Japanese ATM mutation

Introduction

Ataxia-telangiectasia (A-T; MIM# 208900) is an autosomal recessive neurodegenerative disorder characterized by progressive cerebellar degeneration, ocular apraxia and telangiectasia, increased cancer risk, immunodeficiency, sensitivity to ionizing radiation (IR), chromosomal instability, and cell cycle abnormalities [Boder and Sedgwick, 1958; Gatti, 2001]. A-T is caused by mutations in the *ATM* gene (MIM# 607585) that usually encodes a 13 kb transcript that produces a 370 kDa protein [Gatti et al., 1988; Lange et al., 1995; Savitsky et al., 1995]. Intranuclear ATM protein is low or absent in most A-T patients, despite the presence of relatively normal levels of *ATM* transcripts. ATM is activated by autophosphorylation after binding with the MRN (Mre11-Rad50-Nbs) complex at sites of DNA double strand breaks [Bakkenist and Kastan, 2003; Kozlov et al., 2006], and subsequently phosphorylates hundreds of downstream target proteins involved in cell cycle checkpoints, DNA repair, and apoptosis [Bolderson et al., 2009; Matsuoka et al., 2007; Shiloh 2006]. ATM also appears to play a critical role in resolving chronic inflammation [Westbrook and Schiestl, 2010].

A-T patients are usually compound heterozygotes, carrying two distinct mutations. Mutations occur throughout the entire gene without hot spots. Founder effects are commonly observed in many ethnic isolates [Birrell et al., 2005; Campbell et al., 2003; Cavalieri et al., 2006; Gilad et al., 1996a; Laake et al., 1998; McConville et al., 1996; Mitui et al., 2003, 2005; Telatar et al., 1998a, b] wherein patients often carry mutations in a homozygous state. We have previously shown [Du et al., 2007, 2009, 2011; Lai et al., 2004] that accurately analyzing the functional consequences of mutations in individual A-T patients enables the grouping of patients into "mutation categories" that are most likely to be corrected by future customized mutation-targeted therapies.

The aims of the present study were to: (1) characterize the *ATM* mutations in Japanese A-T (JPAT) families; and (2) identify which JPAT patients might be candidates for personalized mutation-targeted therapy. We report that three of eight JPAT families examined are potential candidates for mutation-targeted therapy based on partial restoration of functional ATM protein production.

Materials and Methods

Cell Lines

Lymphoblastoid cell lines (LCLs) [Svedmyr et al., 1975] or activated T-cells [Minegishi et al., 2006] were established from affected

Additional Supporting Information may be found in the online version of this article.

*Correspondence to: Richard A. Gatti, Department of Pathology and Laboratory Medicine, UCLA School of Medicine, 675 Charles E. Young Drive South, Los Angeles, CA 90095-1732. E-mail: rgatti@mednet.ucla.edu

Contract grant sponsors: National Institutes of Health (1R01NS052528); A-T Ease Foundation; A-T Medical Research Foundation.

members of eight Japanese A-T families, including three sibling pairs (JPAT4/5, 8/9, and 11/12). The families came from different geographical regions. Clinical descriptions of patients from these families have been reported previously [Morio et al., 2009].

Short Tandem Repeat (STR) Haplotype Analysis

Standardized STR (short tandem repeat/microsatellite) genotyping for the *ATM* gene region was performed as previously described [Mitui et al., 2003]. Briefly, we used four fluorescently labeled microsatellite markers located within a 1.4 cM region of chromosome 11q22-q23: D11S1819, NS22, D11S2179, and D11S1818. Markers NS22 and D11S2179 are located within the *ATM* gene, in introns 45 and 62, respectively [Udar et al., 1999; Vanagaite et al., 1995]. Allelic sizes were detected with an ABI 3730 DNA analyzer (Applied Biosystems Inc, Carlsbad, CA) and standardized to a reference sample (CEPH 1347-02).

Identification of Mutations

Total RNA was isolated from patient-derived T-cell lines using RNeasy (QIAGEN, Valencia, CA), and cDNA was synthesized using random primers and the Superscript III reverse transcriptase (Invitrogen, Carlsbad, CA). The entire *ATM* coding region was divided into eight overlapping fragments (Regions 1–8) ranging from 1,500 to 1,800 bps [Du et al., 2008]. These regions were PCR amplified and then sequenced using 19 different primers. Mutations on the cDNA level were confirmed in genomic DNA (gDNA) by sequencing relevant exon and intron boundaries. Mutation analysis is based on the same ATM reference sequence used for ATM mutations in the Leiden Open Variation Database (www.LOVD.nl/ATM; NCBI reference sequence:NM_000051.3).

Maximum Entropy Scores and Search for Exonic Splicing Enhancers (ESEs)

The strength of the 5′ and 3′ splice sites (ss) was determined by calculating and comparing the wild-type and mutant 5′ and 3′ ss using the Maximum Entropy software available at http://genes.mit.edu/burgelab/maxent/Xmaxentscan_scoreseq.html [Eng et al., 2004; Mitui et al., 2009; Yeo and Burge, 2004]. We scanned for putative binding motifs for serine/arginine-rich (SR) proteins using the ESEfinder software available at http://rulai.cshl.edu/tools/ESE [Cartegni et al., 2003; Smith et al., 2006].

Long-Range PCR and Breakpoint Regions for Genomic Deletions

To amplify large gDNA fragments, 500 ng of gDNA was used as template, followed by 35 cycles of 95C for 1 min, 68°C for 10 min, and extension at 72°C for 15 min using EX Taq polymerase according to the manufacturer's protocol (Takara Bio Inc, Shiga, Japan). Fragments containing large genomic deletions (LGDs) were isolated from agarose gels and sequenced to determine the breakpoints.

Multiplex Ligation-dependent Probe Amplification (MLPA)

A total of 100 ng of gDNA was used as starting material for the SALSA MLPA P041 and P042 *ATM* kits (MRC-Holland, Amsterdam, Netherlands, www.mrc-holland.com) [Schouten et al., 2002]. The P041 probe mix contained probes for 33 of the 65 exons as well as three probes for exon 1. The P042 *ATM* probe mix contained probes for the remaining *ATM* exons. Both probe mixtures also contained probes for control genes. After hybridization, ligation, and amplification, according to the instructions of the manufacturer, 1 μl of PCR product was mixed with 0.2 μl of ROX-500 labeled internal size standard, separated on an ABI Prism 3100 Avant automatic sequencer (Applera, Norwalk, Connecticut, CA), and analyzed using the GeneScan software ver.3.1. For MLPA data analysis, we used Coffalyser MLPA DAT software developed by MRC-Holland. For each probe, a range from 1 ± 0.2 was considered as a normal exon dosage, while a deletion was determined as being between 0.3 and 0.7.

Antisense Morpholino Oligonucleotide (AMO) Design and Treatment

A 25-mer antisense morpholino oligonucleotide (AMO) was designed to target the 5′ aberrant splice site of a pseudoexon mutation in pre-mRNA of JPAT11/12. The AMO-J11 sequence was: CCTGGAAAAATACTTACAATTAAAC. AMO748C (ATTCACACACTCGAATTCGAAAGTT) and AMO4956GC (CTTGGATAACTGCAACAAATTGACA) were designed to target wild-type sequences to determine potential regulatory elements at the site of a mutation(s). AMOs were synthesized by Gene-Tools (Philomath, OR). Treatment of LCLs with AMOs was performed as previously described [Du et al., 2007]. Cells were suspended in 5% FBS/RPMI medium and the AMO was added directly to medium at the concentrations indicated. Endo-Porter (Gene-Tools) was added to the medium to assist in intracellular incorporation of the AMO. Cells were collected after 48 hr for RNA analysis, and after 84 hr for ATM protein detection. Vivo-AMO was also used to treat JPAT 11 to enhance cellular delivery (Gene-Tools).

Irradiation Induced ATM-Ser1981 Foci Formation (IRIF)

Immunostaining of nuclear foci of ATM-Ser1981was performed as described [Du et al., 2007, 2009]. In brief, LCLs were first treated with the relevant compounds for 4 days before being irradiated with 2 Gy and then incubated at 37°C for 30 min. Next, the cells were fixed with 4% paraformaldehyde and then permeabilized on cover slips. The cover slips were blocked for 1 hr and incubated with mouse anti-ATM pSer1981 for 1 hr (1:500; Cell Signaling Technology, Danvers, MA). After a second blocking, cells were stained with Alexa Fluor 488 anti-mouse IgG (1:150; Invitrogen) for 1 hr and mounted onto slides.

Flow Cytometry Analysis of ATM-Ser1981 Autophosphorylation (FC-ATM-pSer1981)

FC-ATM-pSer1981 was used to verify the restoration of Ser1981 autophosphorylation by readthrough compounds (RTCs) [Du et al., 2009; Nahas et al., 2009]. The cells were treated for 4 days with RTCs, resuspended in PBS, and irradiated with 10 Gy. After 1 hr, the cells were fixed and permeabilized using FIX & PERM (Invitrogen). The cells were then incubated with 1 μl of mouse ATM-s1981 antibody (Cell Signaling Technology) for 2 hr at room temperature. After this time, cells were washed and resuspended in 100-μl PBS with Alexa Fluor 488 anti-mouse IgG (Invitrogen) for 45 min, and then washed and resuspended in PBS with 0.2% paraformaldehyde, before being analyzed using a FACSCalibur (BD, Franklin Lakes, NJ).

Western Blotting

Nuclear extracts were prepared by following the NE-PER protocol (Thermo Fisher Scientific, Rockford, IL). Proteins were separated

on a 7.5% SDS-polyacrylamide gel. Western blots were prepared as described [Du et al., 2007], and probed with anti-ATM (Novus Biologicals, Littleton, CO), -SMC1, or -KAP1 antibodies (Novus Biologicals).

Results

Mutation Analysis

We initially screened our A-T patients for two previously reported Japanese mutations, c.4776(IVS33)+2T>A and c.7883_7887delTTATA [Ejima and Sasaki 1998; Fukao et al., 1998]. Neither of these mutations was detected.

STR genotyping of the *ATM* genomic region was performed for 11 JPAT patients, but since parental gDNAs were unavailable, we could only verify that one patient was homozygous for all markers (JPAT2): [S1819, 131; NS22, 165; S2179, 143; S1818, 162] [Mitui et al., 2003]. As a result, we set out to directly sequence the entire *ATM* coding region after PCR amplifying eight partially overlapping fragments from patients' cDNA [Du et al., 2008]. We identified 12 of the 16 expected mutations (75%) and confirmed them upon sequencing gDNA (Table 1). Only one patient (JPAT2) was homozygous, suggesting that most JPAT patients do not result from consanguineous marriages. The 12 mutations included four frameshifts (counting the homozygous JPAT2 twice), two nonsense, and six splice variants (Table 1). The remaining mutations (4/16; 25%) were four LGDs, which we identified after performing long-range PCR using gDNA as template. Fourteen mutations were novel; two had been previously reported: c.748C>T in JPAT6 [Teraoka et al., 1999] and c.2639-384A>G in JPAT11/12 [Sobeck 2001]. All mutations resulted in the absence of ATM protein (Supp. Fig. S1 and data not shown).

Splicing Mutations

The six splicing mutations identified were analyzed by using Maximum Entropy software (MaxENT) to estimate the strength of the splice sites [Yeo and Burge, 2004] and type of splice defect [Eng et al., 2004]. The mutations found are described below, and diagrams for potential splicing mechanisms are shown in Figure 1.

(1) c.331+5G>A (IVS6): This mutation changed the MaxENT score of the 5′ ss from 9.8 to 3.6. A shorter PCR product compatible with exon 6 skipping was observed at the cDNA level in patient JPAT1 using primers for exons 4 and 7 (Figs. 1 and 2A, lane 3).

(2) c.748C>T: cDNA from patient JPAT6 showed skipping of exon 9 (Figs. 1and 2B, lane 5). This allele with substitution c.748C>T predicted an amino acid change from Arg to a stop codon (CGA >TGA). Given that c.748C>T did not affect the scores for consensus splice sites, nor affect an ESE site, we hypothesized that it affected an as yet unknown splicing regulatory element. To test this idea further, we designed an AMO targeting the wild-type sequence at the site of the mutation in order to block the interaction between any regulatory molecule(s) and the wild-type sequence. Wild-type cells treated with increasing concentrations of AMO748C (Fig. 2G) showed skipping of exon 9, supporting idea model that the region around nucleotide 748 most likely contains a regulatory splicing motif.

(3) c.2639-384A>G (IVS19): The c.2639-384A>G variant in patient JPAT11/12 creates a novel splice acceptor site within IVS19 (Fig. 1), thereby creating a cryptic splice and "pseudo-exon" of 58 bp is created in intron 19 (Fig. 2C, lanes 5 and 6).

Table 1. Mutations of Eight Japanese Families

Ex/Int	Patient	cDNA change	Genomic DNA mutation	Consequence
IVS6	JPAT1[a]	c.186_331del146 (deletes exon 6)	**c.331+5G>A (5′ss 9.81>3.58)**	Aberrant splicing (IV)
7	JPAT6[a]	c.397_398insT	**c.397_398insT**	Frameshift
9	JPAT6[b]	c.663_901del239 (deletes exon 9)	c.748C>T (R>X)	Aberrant splicing (III)
10	JPAT8/9[a]	c.902_1065del164 (deletes exon 10)	**c.902-19_1065+869del1052**	Large genomic deletion
IVS19	JPAT11/12[a]	c.2639_2640ins58	c.2639-384A>G (5′ss 0.36>8.54)	Aberrant splicing (II)
IVS19	JPAT3[a]	c.2639_2838del200 (deletes exon 20)	**c.2639-19_2639-7del13 (3′ss 8.8>3.4)**	Aberrant splicing (IV)
20	JPAT8/9[b]	c.2877C>G	**c.2877C>G (Y>X)**	Nonsense (TAG)
35	JPAT4/5[a]	c.4910_5005del96 (deletes exon 35)	**c.4956GC>TT (LQ>FX)**	Aberrant splicing (III)
38	JPAT1[b]	c.5415G>A	**c.5415G>A (W>X)**	Nonsense (TGA)
IVS48	JPAT11/12[b]	c.6808_7515del708 (deletes ex 49-52)	**c.6807+272_7516-275del5350**	Large genomic deletion
55	JPAT4/5[b]	c.7925_7926del2(GA)	**c.7925delGA**	Frameshift
60	JPAT10[a]	c.8419_8584del166 (deletes exon 60)	**c.8419-643_8507del732**	Large genomic deletion
61	JPAT10[b]	c.8585_8671del87 (deletes exon 61)	**c.8585-1G>C (5′ss 10.2>2.0)**	Aberrant splicing (IV)
61	JPAT2[h]	c.8624delA	**c.8624delA**	Frameshift
IVS63	JPAT3[b]	c.8851_9697del847	**c.8852-2kbdel17kb (CRAT [B] mutation?)**	Large genomic deletion

Bolded mutations have not been reported previously.
[a]First allele.
[b]Second allele.
[h]Homozygote.
Nucleotide numbering is based on +1 being the A of the first translation start codon in exon 4 (NCBI reference sequence: NM_000051.3).

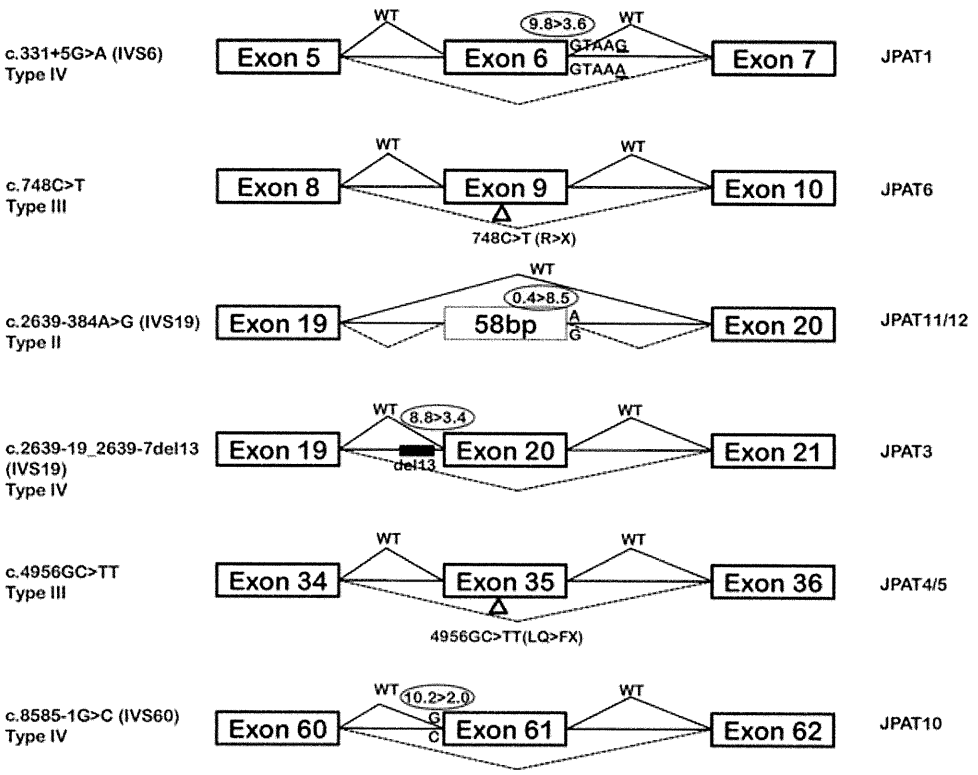

Figure 1. *ATM* splicing mutations. Genomic mutations causing splicing mutations were analyzed for changes in splicing scores calculated by Max ENT. Classification of splicing mutations is reported accordingly to Eng et al. [2004]. See text for additional details.

This results in a frameshift and a predicted secondary premature stop codon.

(4) c.2639-19_2639-7del13 (IVS19): In Figure 2D (lane 3), the PCR products from JPAT3 cDNA showed a normal and an additional prominent lower band (783 bp and 583 bp, respectively). Sequencing of the 583-bp band revealed skipping of exon 20. gDNA sequencing identified a 13 nt deletion in intron 19 at position c.2639-19_2639-7. The 3′ MaxENT score changed from 8.8 to 3.4 (Fig. 1).

(5) c.4956GC>TT: In family JPAT4/5, we identified a c.4956GC>TT substitution within exon 35 (p.LQ1652_1653FX) that leads to skipping of exon 35 without affecting an ESE or canonical splice sites (Figs. 1 and 2E, lanes 3 and 4). Exposing wild-type LCLs to increasing concentrations of AMO4956GC, targeting the mutation site, revealed skipping of exon 35 (Fig. 2H); these results suggest that nucleotide 4956 is part of a regulatory protein binding site, which when disrupted influences the aberrant splicing observed in JPAT4/5.

(6) c.8585-1G>C (IVS60): JPAT10 harbors the IVS60-1G>C mutation that changed the MaxENT score of the 3′ ss from 10.2 to 2.0, resulting in a skipping of the exon 61 (Fig. 2F, lane 4). Interestingly, the second allele of this patient was a splicing mutation that is predicted to result in exon 60 skipping (Fig. 2F, lane 4). We sequenced gDNA for exons 59–62 but failed to find a mutation that would account for the skipping of exon 60 (however, see additional results on JPAT10 below).

Large Genomic Deletions (LGDs)

(1) c.902-19_1065+869del1052 (del ex10): Two siblings (JPAT8/9) yielded an abnormal 369-bp fragment when cDNA was amplified from exon 9 to 11 (Fig. 3A, cDNA gel, lanes 3 and 4). When this band was isolated and sequenced, we found a deletion of exon 10. No mutation was observed in exons 9–11, ruling out a conventional splicing mutation. Using long-range PCR to amplify the genomic region from exon 9 to 11, we obtained a 3.3 kb fragment (Fig. 3A, gDNA gel lanes 3 and 4), whose sequence revealed a 1,052-bp deletion from IVS9-19 to IVS10+869; this deletion included exon 10 (164 bp).

(2) c.6807+272_7516-275del5350 (del ex49-52): Two siblings (JPAT11/12) showed an abnormal PCR fragment of 1.1 kb when cDNA was amplified from exon 48 to 53 (Fig. 3B, cDNA gel). The sequence of the PCR product showed a deletion of exons 49–52. A long-range PCR performed on gDNA using primers for exons 48 and 53 produced a 1.1 kb band instead of the expected 6.4 kb (Fig. 3B, left). Sequencing of the 1.1 kb band revealed a 5,350-bp genomic deletion that starts in intron 48 and ends in intron 52.

(3) c.8419-643_8507del732 (del ex 60): In patient JPAT10, we suspected that skipping of exon 60 might reflect an LGD. We amplified the gDNA surrounding exons 59–61 and found a 732-bp genomic deletion extending from IVS59-643 to nucleotide 89 of exon 60 (Fig. 3C).

(4) c.8851-2kbdel17kb (del ex64-65): When mutation screening failed to identify a second pathogenic mutation in JPAT3, we were prompted to search for an LGD mutation with Multiplex Ligation-dependent Probe Amplification (MLPA). We observed a significant decrease in peak height for the final exons 64 and 65, indicative of a deletion carried in heterozygous state (Fig. 4A). Previous studies have demonstrated two LINE-1 sequences between IVS63 and downstream of exon 65, as well as a 17 kb genomic deletion in the *ATM* gene of A-T patients

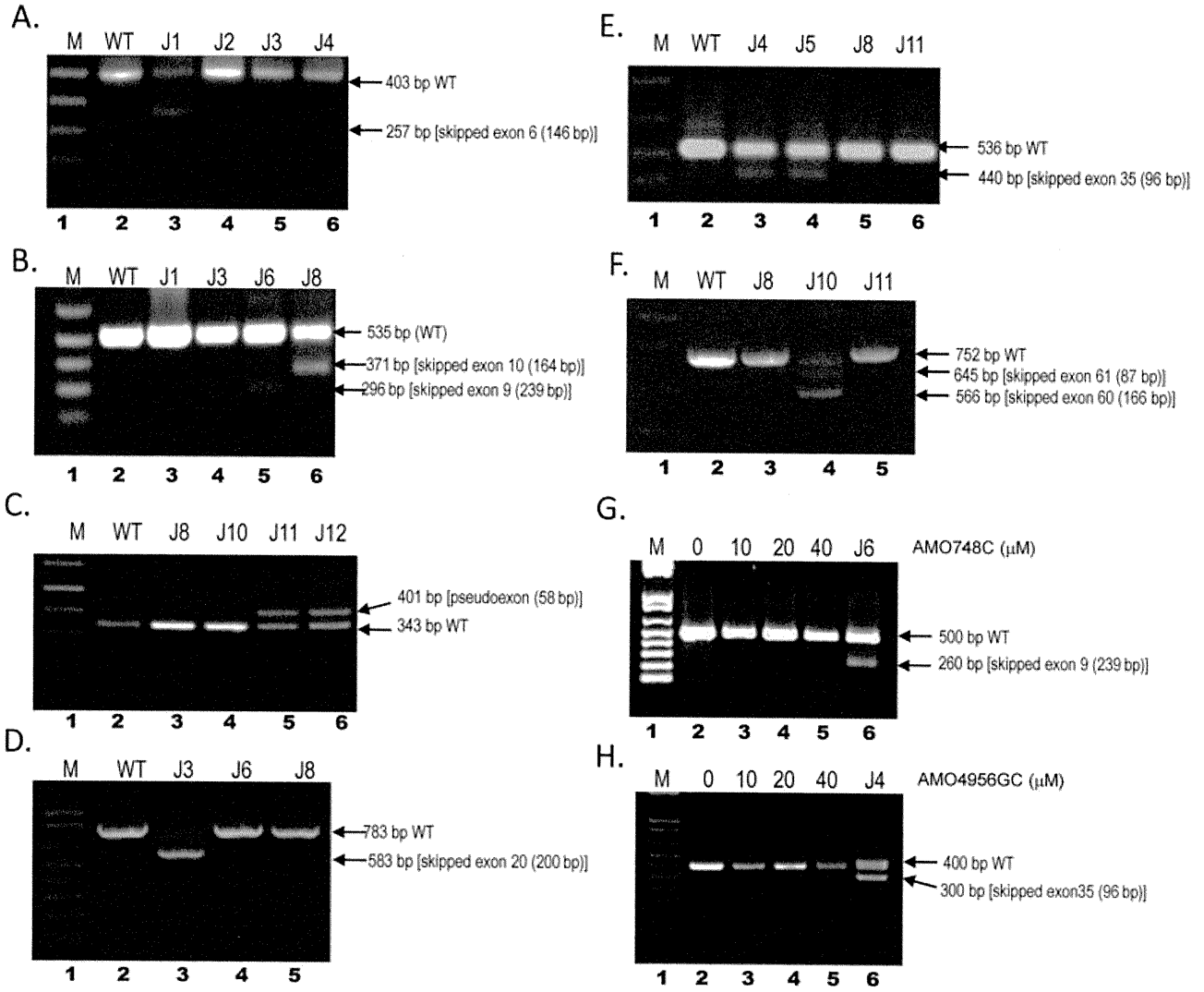

Figure 2. Effect of splicing mutations on cDNA. Agarose gel images of PCR products showed aberrant spliced products. Patient cDNA were used as templates for PCR amplifications in the regions displaying splicing mutations. M (lane 1) is 1 kb plus ladder (Invitrogen), wild-type cDNA was used as control (lane 2). **(A)** Skipped exon 6 in JPAT1 (lane 3). **(B)** Skipped exon 9 in JPAT6 (lane 5) and skipped exon 10 in JPAT8 (lane 6). **(C)** Pseudoexon of JPAT11 and JPAT12 (lanes 5 and 6). **(D)** Skipped exon 20 in JPAT3 (lane 3). **(E)** Skipped exon 35 in JPAT4 and JPAT5 (lanes 3 and 4). **(F)** Skipped exons 60 and 61 in JPAT10 (lane 4). **(G)** AMO-treated wild-type lymphoblastoid cell line (LCL) produced alternative spliced product that skipped exon 9. JPAT6, carrying the c.748C>T mutation, showed a skipped exon 9 product (lane 6), **(H)** AMO 4956GC treated wild-type LCL produced alternative spliced product that skipped exon 35. JPAT4 that has 4956GC>TT mutation showing skipped exon 35 products as a control (lane 6). See text for additional details.

with Costa Rican, Dutch, and Brazilian backgrounds [Broeks et al., 1998; Coutinho et al., 2004; Mitui et al., 2003; Telatar et al., 1998b].

Figure 4B summarizes the locations of primers, LINE-1 sequences, and an LGD for this region.

We used two sets of primers: Primer set #1 (P1Fw and P4Rev) was 23 kb apart, flanking the 17 kb deletion. Because of the nature of our PCR conditions, no PCR product was anticipated from the wild-type allele, while the mutant allele should yield a 6 kb fragment. Primer set #2 (P2Fw and P3Rev) was placed within the 17 kb deletion, which should have produced a 2.4 kb fragment from only the wild-type allele [Telatar et al., 1998b]. Figure 4B (lane 2) shows that wild-type gDNA produced the 2.4 kb fragment, while CRAT [B] (a Costa Rican patient homozygous for a 17 kb deletion) produced the 6 kb fragment (lane 4). A CRAT [B] heterozygote produced both the 2.4 kb fragment and the 6 kb product from the deletion (Fig. 4B, lane 5). The CRAT [B] band pattern was also observed in the gDNA of JPAT3, suggesting the presence of an LGD between two LINE-1 sequences (Fig. 4B, lane 3). Available breakpoints and surrounding sequences were analyzed using Repeat Masker software to search for flanking repetitive elements [Babushok and Kazazian, 2007; Kazazian and Goodier, 2002; Telatar et al., 1998b] (see Fig. 3). Because the breakpoint was in a highly homologous repeat sequence, the ends could not be accurately determined. The other Japanese patient (JPAT8) who did not have a deletion in this region showed a pattern identical to the wild type (Fig. 4B, lane 6).

The STR haplotypes for JPAT3, CRAT [B], and BRAT3 differed. JPAT3: S1819 [131,133]; NS22 [173,175]; S2179 [137,137]; S1818 [160,168]; CRAT [B]: S1819 [131]; NS22 [171]; S2179 [141]; S1818 [160] [Mitui et al., 2003]; BRAT 3: S1819 [133]; NS22 [155]; S2179

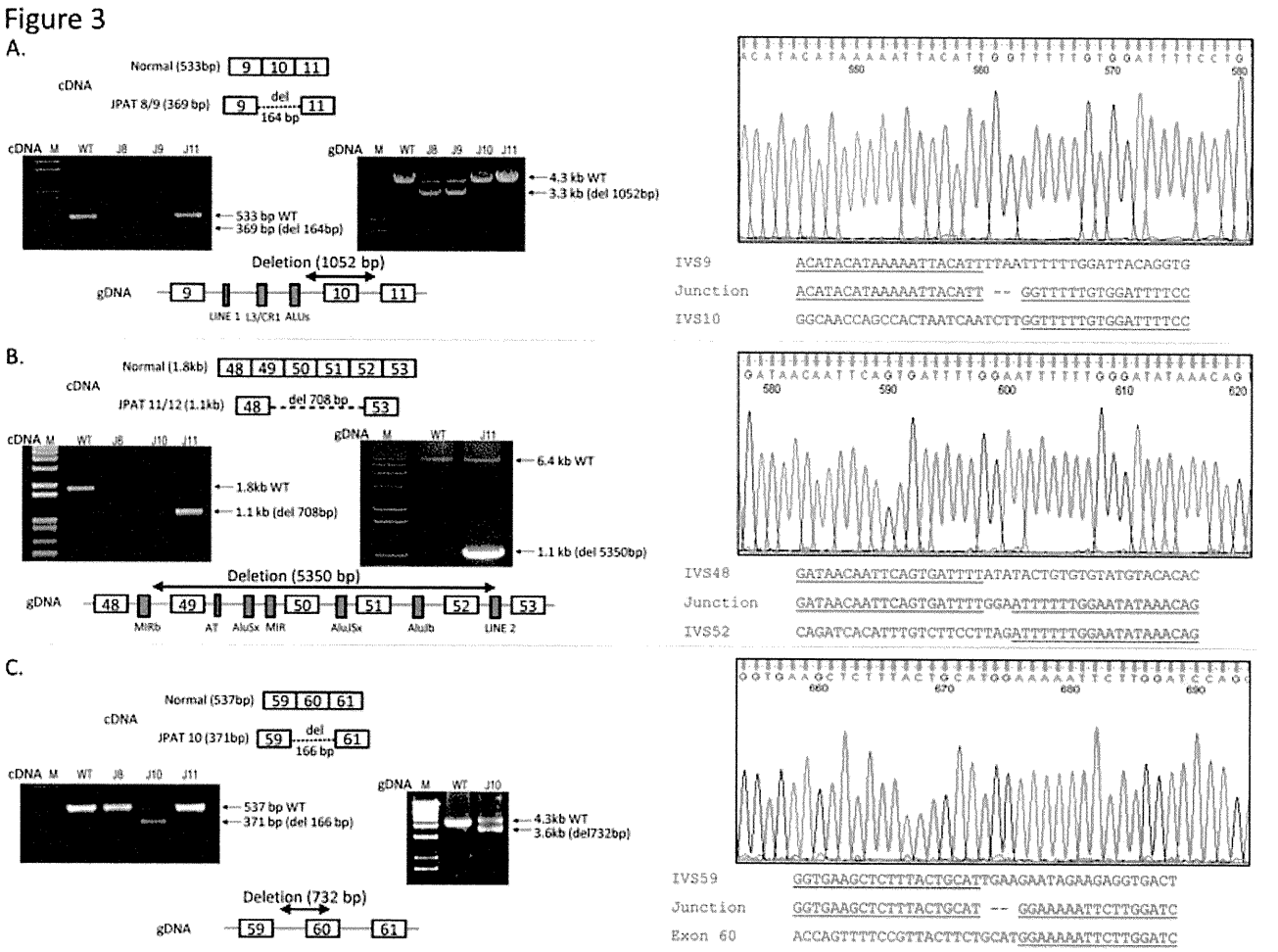

Figure 3. Large genomic deletions (LGDs). **(A)** Schematic representation of cDNA showing deletion of exon 10 and agarose gel image of PCR products (using primers GFw and GRev) (left): Lane 1 is 1 kb plus ladder (Invitrogen), lane 2 is wild-type control, lane 3 (JPAT8) and lane 4 (JPAT9) showing deletion of exon 10, lane 5 is JPAT control. Agarose gel image (right) for genomic DNA (gDNA) PCR products (using primers EX9Fw and EX11Rev) showing deletion of 1 kb in JPAT8/9. Schematic representation of DNA shows LGD, as well as repetitive elements within the region (at bottom). Sequence data with junction sequences are shown on right. **(B)** Schematic representation of cDNA change in JPAT11/12 between exon 48 and exon 53, which are analyzed by PCR (using primers FATFw and FATRev). Agarose gel image (left) for cDNA shows aberrant spliced products of JPAT11 (lane 5). Lane 1 is 1 kb plus ladder, lane 2 is wild-type, lanes 3 and 4 are JPAT control. Agarose gel image (right) for gDNA shows deletion of 5.3 kb (using EX Taq polymerase with LREX48Fw and LREX53Rev primers). Schematic representation of gDNA (at bottom) shows large deletion. Sequence data with junction sequences are shown on right. **(C)** Schematic representation of JPAT10 cDNA shows deletion of exon 60. Agarose gel image (left) shows aberrant spliced products. Agarose gel image (right) for gDNA PCR products (using primers EX59Fw and EX61Rev) show reduced size in JPAT10 (3.6 kb) compared to wild type (4.3 kb) and schematic representation of gDNA showing deletion at c.8269-643del732, which includes the first 89 bp of exon 60. Sequences are shown at right.

[147]; S1818 [146] [Mitui et al., 2003]. These results suggested that the c.8851-2kbdel17kb mutations in the three patients were not ancestrally related.

Correction of Type II Pseudoexon Splicing Mutation using an AMO

In family JPAT11/12, we identified a type II splicing mutation [Eng et al., 2004] c.2639-384A>G, which created a cryptic acceptor splice site resulting in the inclusion of 58 bp of intronic sequence (Figs. 2C and 5A). We designed AMO-J11 to target the cryptic 5′ splice site (Fig. 5A) [Du et al., 2007; Eng et al., 2004]. The LCL of JPAT11 was treated with AMO-J11 for 4 days followed by RT-PCR analysis. Mutant splicing was almost completely abrogated in an AMO dose-dependent manner and normal transcript was restored (Fig. 5B). Nuclear extracts from treated JPAT11 cells also showed a full-length ATM protein (data not shown). In order to enhance the delivery and efficiency of the AMO, we also designed a structurally modified AMO referred as "Vivo-AMO" [Morcos et al., 2008; Moulton and Jiang, 2009]. Notably, a significant amount of functional ATM protein was induced by 0.5 μM Vivo AMO-J11 (Fig. 5C). However, "Vivo-AMO" started to show possible cytotoxicity at 0.8μM (Fig. 5C, lane 4).

Correction of Nonsense Mutation in JPAT8 using RTCs

The JPAT8/9 siblings lack ATM protein because they carry an LGD and a nonsense mutation (c.2877C>G, p.Tyr959X). Functional ATM protein is inducible with compounds that readthrough premature termination codons [Du et al., 2009] even when the LCL carries the nonsense mutation in a heterozygous state [Lai et al., 2004]. We treated JPAT8 LCL with the readthrough compound RTC13 for 4

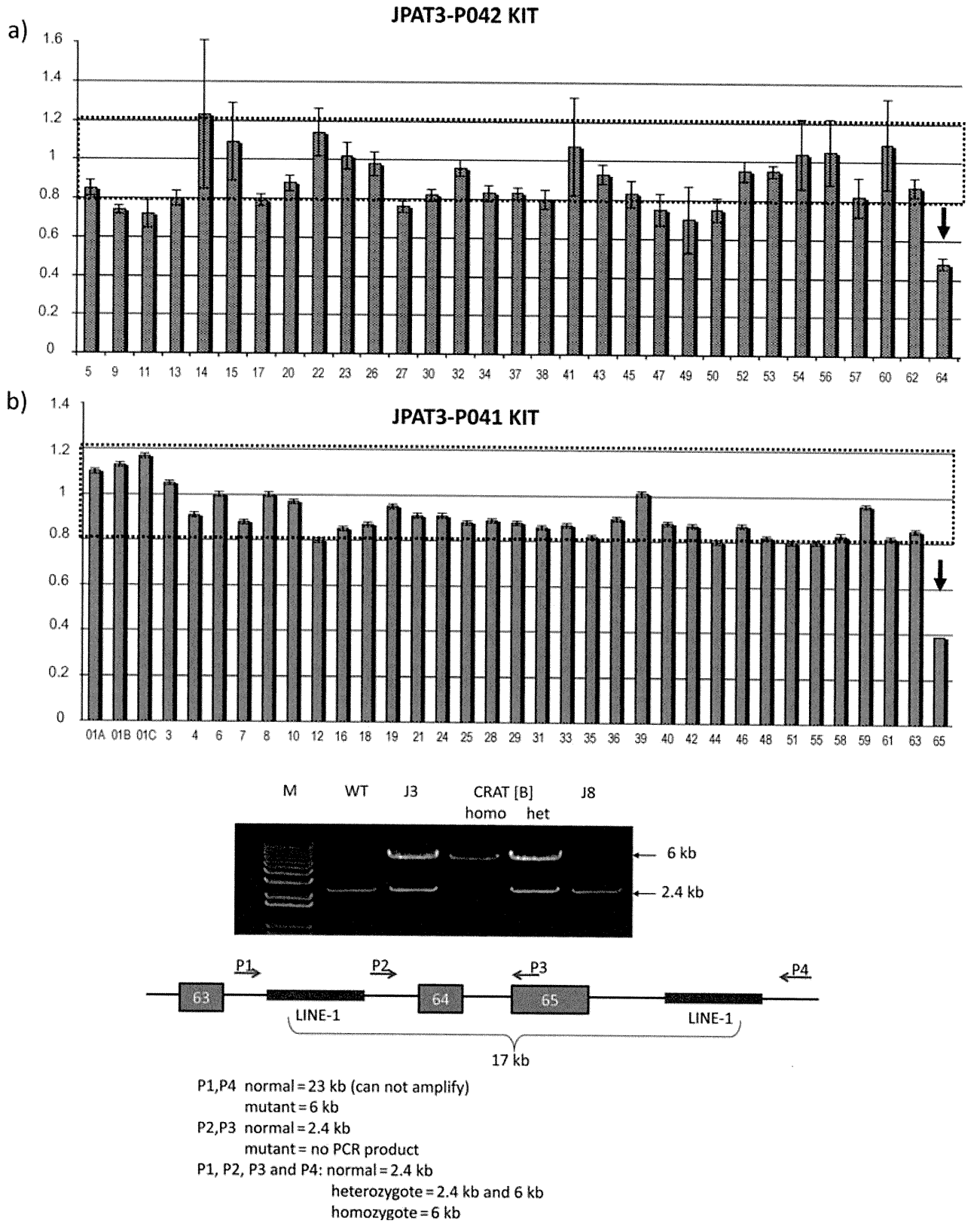

Figure 4. Analysis of LGD in patient JPAT3. **(A)** Multiplex Ligation Probe Amplification (MLPA) analysis using MLPA P041 **(A)** and P042 **(B)** kits. For each of the two analyses normalized peak area histograms of JPAT3 are shown. The dotted lines indicate the normal exon dosages between 0.8 and 1.2. The heavy black arrows indicate the exon probes of decreased signal, corresponding to the genomic deletion of exons 64 and 65. **(B)** PCR products depicting a LGD between two LINE-1 sequences. Lane 1 is 1 kb plus ladder, lane 2 is wild-type control, lane 3 is JPAT3, lane 4 is homozygous CRAT [B] patient with a very similar mutation, lane 5 is a heterozygous individual with CRAT [B] mutation, lane 6 is JPAT8. Schematic diagram (below) shows the relative locations for four different primers at the region of the LGD.

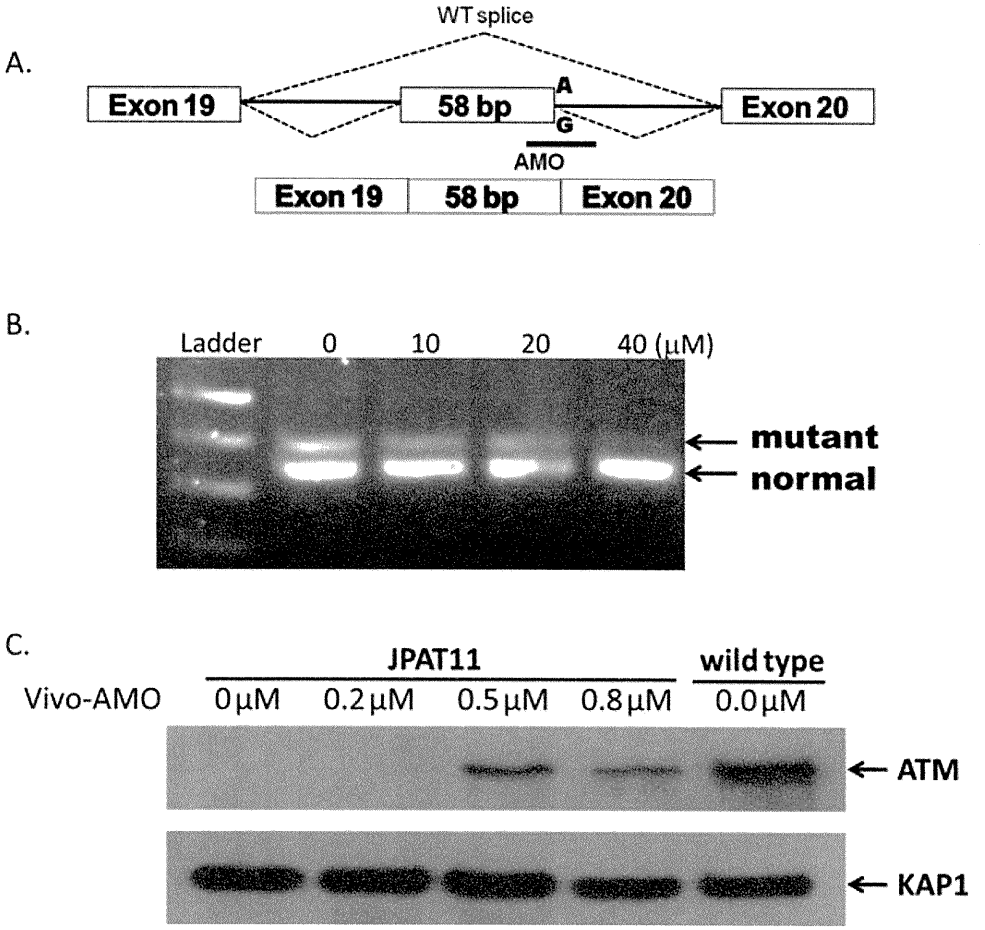

Figure 5. Correction of a splicing mutation in JPAT11 using AMO-J11. **(A)** Schematic representation of inclusion of pseudoexon (type II) and location of designed AMO. **(B)** JPAT11 cells were treated with 0, 10, 20, and 40 μM AMO for 4 days and RNAs were isolated and analyzed for corrected splicing products. **(C)** JPAT11 cells were treated with 0.2, 0.5, and 0.8 μM of Vivo-AMO-J11 for 4 days and nuclear lysates were isolated for western blotting. KAP1 antibody was used as a loading control.

days, and measured ATM autophosphorylation after DNA damage induced by IR. An aminoglycoside RTC, G418, served as a positive control. Both G418 and RTC13 successfully induced ATMpS1981 autophosphorylation as shown by (A) FC-ATMpSer1981 and (B) IRIF ATMpSer1981 assays (Fig. 6), thereby demonstrating a potential therapeutic approach for these siblings, despite the presence of a nonsense mutation in only one allele.

Discussion

Whereas a high (0.5%) coefficient of inbreeding had been recorded for the Japanese population [Pattison, 2004], the *ATM* mutation spectrum identified in our JPAT patient cohort included almost no homozygous mutations and no founder mutations. The c.4776+2T>A and c.7883_7887del5 mutations reported by Ejima and Sasaki [1998] and Fukao et al. [1998] were not observed. In fact, all mutations detected in the JPAT families—four frameshift, two nonsense, four LGDs, and six affecting splicing—were new except for a previously identified c.748C>T splicing mutation in an Irish–American family [Teraoka et al., 1999] and the c.2639-384A>G mutation [Sobeck, 2001]. It is noteworthy that only three of the six splicing mutations involved canonical sites (c.331+5G>A, c.2639-19_2639-7del13, c.8585-1G>C). In the other mutations: (1) c.748C>T (exon 9) and 4956GC>TT (exon 35) presented as nonsense mutations in gDNA, but at the cDNA level caused skipping of the exon in which they were located; and (2) JPAT11/12 had a deep-intronic mutation (c.2639-384A>G) in intron 19 that seemed to activate a cryptic acceptor splice site resulting in the insertion of a 58-bp pseudoexon in the transcript (Figs. 1, 2C, and 5).

Nonsense mutations frequently alter the splicing of the exon containing them, an observation that has been termed nonsense-associated altered splicing (NAS) [Valentine, 1998]. In most cases of NAS, the mutation disrupts an ESE critical for exon inclusion [Liu et al., 2001]. AMOs usually act by covering/masking a mutated site in the pre-mRNA, but cannot be used to correct splicing mutations at canonical sites. Thus, AMOs are most effective in correcting type II and IV splice mutations [Eng et al., 2004]. Most relevant here, AMOs can be applied to the functional analysis of *ATM* mutations. By using AMOs designed to bind the wild-type exon 9 and exon 35 sequences located around the mutation sites, we were able to induce alternative splicing (Fig. 2G and H). These results suggest that unknown regulatory elements are probably located near or at the sites of the mutation and are necessary for modulating normal splicing events in these exons. Furthermore, as described earlier, the deep-intronic mutation (c.2639-384A>G) in intron 19 is among the most attractive candidates for AMO therapy (Fig. 5) [Du et al., 2007].

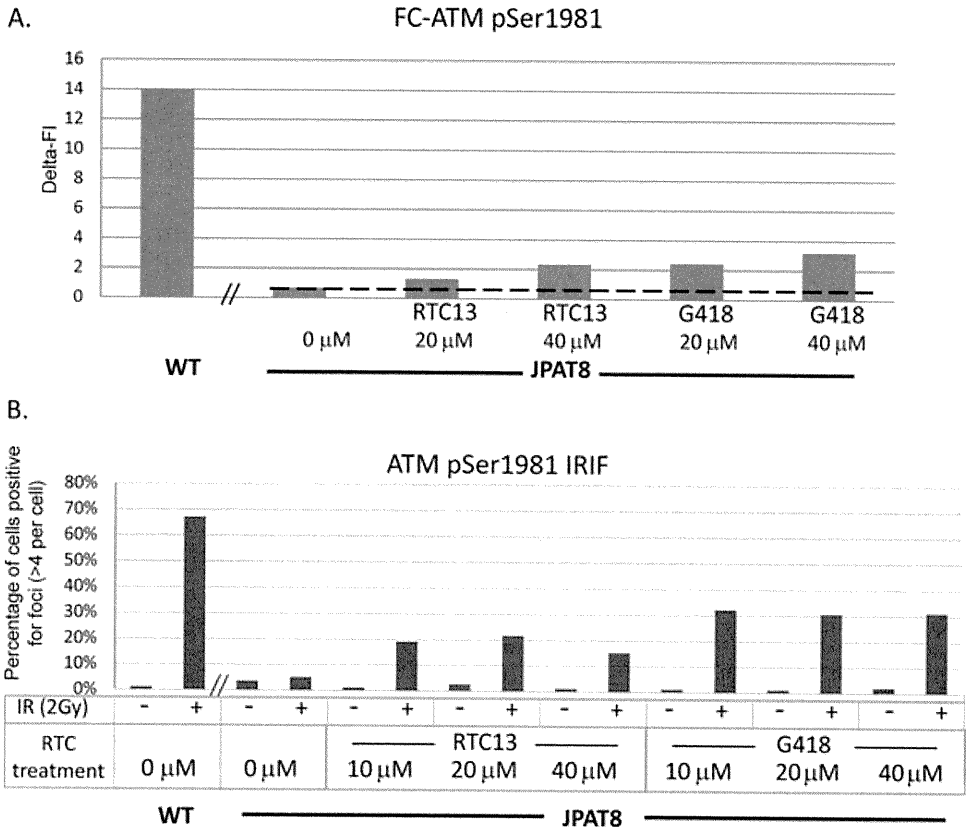

Figure 6. Readthrough compounds (RTCs) restored ATMpSer1981 autophosphorylation in JPAT8 LCL with a nonsense mutation. Cells were treated with readthrough compounds RTC13 and G418 for 4 days and then analyzed for ATMpSer1981. **(A)** ATMpSer1981 autophosphorylation level measured by FC-ATMpSer1981. Delta FI (fluorescence intensity) reflects the difference in FI between nonirradiated and irradiated cells. The data represent one of three independent experiments and results were consistent. **(B)** ATMpSer1981 foci formation by IRIF assay. The data are an average of two independent experiments.

LGDs and duplications within the *ATM* gene account for approximately 2% of reported mutations [Cavalieri et al., 2006, 2008; Coutinho, et al., 2004; Ejima and Sasaki, 1998; Gilad et al., 1996b; Mitui et al., 2003; Telatar et al., 1998b]. Few LGDs have been found in a homozygous state in A-T patients [Mitui et al., 2003]. The recent introduction of the MLPA technique has greatly improved the detection of genomic rearrangement mutations, including LGD and duplications in the *ATM* gene [Cavalieri et al., 2008].

Using MLPA, we identified the c.8851-2kbdel17kb mutation in JPAT3. While it was possible that this LGD mutation was ancestrally related to the previously reported CRAT [B] [Telatar et al., 1998a] and BRAT3 [Mitui et al., 2003] mutations, this now seems unlikely, since all three alleles are carried on different STR haplotypes. Given that homology between repetitive sequences is thought to underlie the formation of some genomic deletions and duplications [Kazazian and Goodier, 2002; Telatar et al., 1998a], we carried out an in silico analysis of DNA sequences flanking genomic deletions and were able to identify several repetitive sequences. The presence of microhomology (GGA in JPAT11) suggests that the recently described microhomology-mediated break-induced replication FoSTeS/MMBIR mechanism could be responsible for generating these deletions [Hastings et al., 2009].

Readthrough of PTCs was first described almost 50 years ago when it was noticed that certain aminoglycosides, such as streptomycin and gentamicin, "suppressed" the mutated phenotype of auxotrophy in strains of *Escherichia coli* suggesting that the drug interfered with accurate translation of the RNA code into protein [Davies et al., 1965]. Later, crystallography studies elegantly demonstrated that aminoglycosides bind to the internal loop of helix 44 (the decoding site) of the 16 S ribosomal RNA [Dibrov et al., 2010; Lynch et al., 2003]. More recently, we identified two new nonaminoglycoside small molecules with readthrough activity on both *ATM* and *dystrophin* genes [Du et al., 2009].

Based on the mutation spectrum of *ATM*, it is estimated that approximately 30% of *ATM* mutations in A-T patients are potentially treatable by mutation-targeted therapy using either RTCs or AMOs. This includes A-T patients who are compound heterozygotes, since RTCs and AMOs restore significant amounts of ATM protein even when only one allele is targeted. We identified three such examples amongst the eight Japanese families. In fact, in vitro, we were able to correct (1) abnormal splicing for JPAT11/12 (Fig. 5A), using a custom-designed AMO to mask the cryptic splice site created by the pseudoexon mutation (c.2639-384A>G); (2) a nonsense mutation in cells from JPAT8/9 using RTCs (Fig. 6). Thus, our results demonstrate that mutation-targeted treatment of cells carrying poorly understood DNA variants can extend our understanding of the consequences of such changes and may also have important therapeutic potential.

Acknowledgments

S.C. received a fellowship from "Associazione Gli Amici di Valentina." We thank Drs. Shareef Nahas, Hailiang Hu, and Mark Ambrose for helpful discussions.

References

Babushok DV, Kazazian HH, Jr. 2007. Progress in understanding the biology of the human mutagen LINE-1. Hum Mutat 28:527–539.

Bakkenist CJ, Kastan MB. 2003. DNA damage activates ATM through intermolecular autophosphorylation and dimer dissociation. Nature 421:499–506.

Birrell GW, Kneebone K, Nefedov M, Nefedova E, Jartsev MN, Mitsui M, Gatti RA, Lavin MF. 2005. ATM mutations, haplotype analysis, and immunological status of Russian patients with ataxia telangiectasia. Hum Mutat 25:593–601.

Boder E, Sedgwick RP. 1958. Ataxia-telangiectasia; a familial syndrome of progressive cerebellar ataxia, oculocutaneous telangiectasia and frequent pulmonary infection. Pediatrics 21:526–554.

Bolderson E, Richard DJ, Zhou BB, Khanna KK. 2009. Recent advances in cancer therapy targeting proteins involved in DNA double-strand break repair. Clin Cancer Res 15:6314–6320.

Broeks A, de Klein A, Floore AN, Muijtjens M, Kleijer WJ, Jaspers NG, van 't Veer LJ. 1998. ATM germline mutations in classical ataxia-telangiectasia patients in the Dutch population. Hum Mutat 12:330–337.

Campbell C, Mitui M, Eng L, Coutinho G, Thorstenson Y, Gatti RA. 2003. ATM mutations on distinct SNP and STR haplotypes in ataxia-telangiectasia patients of differing ethnicities reveal ancestral founder effects. Hum Mutat 21:80–85.

Cartegni L, Wang J, Zhu Z, Zhang MQ, Krainer AR. 2003. ESEfinder: a web resource to identify exonic splicing enhancers. Nucleic Acids Res 31:3568–3571.

Cavalieri S, Funaro A, Pappi P, Migone N, Gatti RA, Brusco A. 2008. Large genomic mutations within the ATM gene detected by MLPA, including a duplication of 41 kb from exon 4 to 20. Ann Hum Genet 72(Pt 1):10–18.

Cavalieri S, Funaro A, Porcedda P, Turinetto V, Migone N, Gatti RA, Brusco A. 2006. ATM mutations in Italian families with ataxia telangiectasia include two distinct large genomic deletions. Hum Mutat 27:1061–1070.

Coutinho G, Mitui M, Campbell C, Costa Carvalho BT, Nahas S, Sun X, Huo Y, Lai CH, Thorstenson Y, Tanouye R, Raskin S, Kim CA, Llerena J Jr, Gatti RA. 2004. Five haplotypes account for fifty-five percent of ATM mutations in Brazilian patients with ataxia telangiectasia: seven new mutations. Am J Med Genet A 126:33–40.

Davies J, Gorini L, Davis BD. 1965. Misreading of RNA codewords induced by aminoglycoside antibiotics. Mol Pharmacol 1:93–106.

Dibrov SM, Parsons J, Hermann T. 2010. A model for the study of ligand binding to the ribosomal RNA helix h44. Nucleic Acids Res 38:4458–4465.

Du L, Damoiseaux R, Nahas S, Gao K, Hu H, Pollard JM, Goldstine J, Jung ME, Henning SM, Bertoni C, Gatti RA. 2009. Nonaminoglycoside compounds induce readthrough of nonsense mutations. J Exp Med 206:2285–2297.

Du L, Kayali R, Bertoni C, Fike F, Hu H, Iversen PL, Gatti RA. 2011. Arginine-rich cell-penetrating peptide dramatically enhances AMO-mediated ATM aberrant splicing correction and enables delivery to brain and cerebellum. Hum Mol Genet 20:3151–3160.

Du L, Lai CH, Concannon P, Gatti RA. 2008. Rapid screen for truncating ATM mutations by PTT-ELISA. Mutat Res 640:139–144.

Du L, Pollard JM, Gatti RA. 2007. Correction of prototypic ATM splicing mutations and aberrant ATM function with antisense morpholino oligonucleotides. Proc Natl Acad Sci USA 104:6007–6012.

Ejima Y, Sasaki MS. 1998. Mutations of the ATM gene detected in Japanese ataxia-telangiectasia patients: possible preponderance of the two founder mutations 4612del165 and 7883del5. Hum Genet 102:403–408.

Eng L, Coutinho G, Nahas S, Yeo G, Tanouye R, Babaei M, Dork T, Burge C, Gatti RA. 2004. Nonclassical splicing mutations in the coding and noncoding regions of the ATM Gene: maximum entropy estimates of splice junction strengths. Hum Mutat 23:67–76.

Fukao T, Song XQ, Yoshida T, Tashita H, Kaneko H, Teramoto T, Inoue R, Katamura K, Mayumi M, Hiratani M and others. 1998. Ataxia-telangiectasia in the Japanese population: identification of R1917X, W2491R, R2909G, IVS33+2T–>A, and 7883del5, the latter two being relatively common mutations. Hum Mutat 12:338–343.

Gatti RA. 2001. Ataxia-telangiectasia. In: Scriver CR, Beaudet AL, Sly WS, Valle D, editors. The Metabolic and Molecular Basis of Inherited Disease. Edition 8. New York: McGraw-Hill 677–704.

Gatti RA, Berkel I, Boder E, Braedt G, Charmley P, Concannon P, Ersoy F, Foroud T, Jaspers NG, Lange K and others. 1988. Localization of an ataxia-telangiectasia gene to chromosome 11q22–23. Nature 336:577–580.

Gilad S, Bar-Shira A, Harnik R, Shkedy D, Ziv Y, Khosravi R, Brown K, Vanagaite L, Xu G, Frydman M, and others. 1996a. Ataxia-telangiectasia: founder effect among north African Jews. Hum Mol Genet 5:2033–2037.

Gilad S, Khosravi R, Shkedy D, Uziel T, Ziv Y, Savitsky K, Rotman G, Smith S, Chessa L, Jorgensen TJ and others. 1996b. Predominance of null mutations in ataxia-telangiectasia. Hum Mol Genet 5:433–439.

Hastings PJ, Ira G, Lupski JR. 2009. A microhomology-mediated break-induced replication model for the origin of human copy number variation. PLoS Genet 5:e1000327.

Kazazian HH, Jr., Goodier JL. 2002. LINE drive. Retrotransposition and genome instability. Cell 110:277–280.

Kozlov SV, Graham ME, Peng C, Chen P, Robinson PJ, Lavin MF. 2006. Involvement of novel autophosphorylation sites in ATM activation. EMBO J 25:3504–3514.

Laake K, Telatar M, Geitvik GA, Hansen RO, Heiberg A, Andresen AM, Gatti R, Borresen-Dale AL. 1998. Identical mutation in 55% of the ATM alleles in 11 Norwegian AT families: evidence for a founder effect. Eur J Hum Genet 6:235–244.

Lai CH, Chun HH, Nahas SA, Mitui M, Gamo KM, Du L, Gatti RA. 2004. Correction of ATM gene function by aminoglycoside-induced read-through of premature termination codons. Proc Natl Acad Sci USA 101:15676–15681.

Lange E, Borresen AL, Chen X, Chessa L, Chiplunkar S, Concannon P, Dandekar S, Gerken S, Lange K, Liang T and others. 1995. Localization of an ataxia-telangiectasia gene to an approximately 500-kb interval on chromosome 11q23.1: linkage analysis of 176 families by an international consortium. Am J Hum Genet 57:112–119.

Liu HX, Cartegni L, Zhang MQ, Krainer AR. 2001. A mechanism for exon skipping caused by nonsense or missense mutations in BRCA1 and other genes. Nat Genet 27:55–58.

Lynch SR, Gonzalez RL, Puglisi JD. 2003. Comparison of X-ray crystal structure of the 30S subunit-antibiotic complex with NMR structure of decoding site oligonucleotide-paromomycin complex. Structure 11:43–53.

Matsuoka S, Ballif BA, Smogorzewska A, McDonald ER, 3rd, Hurov KE, Luo J, Bakalarski CE, Zhao Z, Solimini N, Lerenthal Y and others. 2007. ATM and ATR substrate analysis reveals extensive protein networks responsive to DNA damage. Science 316:1160–1166.

McConville CM, Stankovic T, Byrd PJ, McGuire GM, Yao QY, Lennox GG, Taylor MR. 1996. Mutations associated with variant phenotypes in ataxia-telangiectasia. Am J Hum Genet 59:320–330.

Minegishi Y, Saito M, Morio T, Watanabe K, Agematsu K, Tsuchiya S, Takada H, Hara T, Kawamura N, Ariga T and others. 2006. Human tyrosine kinase 2 deficiency reveals its requisite roles in multiple cytokine signals involved in innate and acquired immunity. Immunity 25:745–755.

Mitui M, Bernatowska E, Pietrucha B, Piotrowska-Jastrzebska J, Eng L, Nahas S, Teraoka S, Sholty G, Purayidom A, Concannon P and others. 2005. ATM gene founder haplotypes and associated mutations in Polish families with ataxia-telangiectasia. Ann Hum Genet 69(Pt 6):657–664.

Mitui M, Campbell C, Coutinho G, Sun X, Lai CH, Thorstenson Y, Castellvi-Bel S, Fernandez L, Monros E, Carvalho BT and others. 2003. Independent mutational events are rare in the ATM gene: haplotype prescreening enhances mutation detection rate. Hum Mutat 22:43–50.

Mitui M, Nahas SA, Du LT, Yang Z, Lai CH, Nakamura K, Arroyo S, Scott S, Purayidom A, Concannon P and others. 2009. Functional and computational assessment of missense variants in the ataxia-telangiectasia mutated (ATM) gene: mutations with increased cancer risk. Hum Mutat 30:12–21.

Morcos PA, Li Y, Jiang S. 2008. Vivo-Morpholinos: a non-peptide transporter delivers Morpholinos into a wide array of mouse tissues. Biotechniques 45:613–614, 616, 618 passim.

Morio T, Takahashi N, Watanabe F, Honda F, Sato M, Takagi M, Imadome K, Miyawaki T, Delia D, Nakamura K and others. 2009. Phenotypic variations between affected siblings with ataxia-telangiectasia: ataxia-telangiectasia in Japan. Int J Hematol 90:455–462.

Moulton JD, Jiang S. 2009. Gene knockdowns in adult animals: PPMOs and vivo-morpholinos. Molecules 14:1304–1323.

Nahas SA, Butch AW, Du L, Gatti RA. 2009. Rapid flow cytometry-based structural maintenance of chromosomes 1 (SMC1) phosphorylation assay for identification of ataxia-telangiectasia homozygotes and heterozygotes. Clin Chem 55:463–472.

Pattison JE. 2004. A comparison of inbreeding rates in India, Japan, Europe and China. HOMO—J Comp Hum Biol 55:113–128.

Savitsky K, Bar-Shira A, Gilad S, Rotman G, Ziv Y, Vanagaite L, Tagle DA, Smith S, Uziel T, Sfez S and others. 1995. A single ataxia telangiectasia gene with a product similar to PI-3 kinase. Science 268:1749–1753.

Schouten JP, McElgunn CJ, Waaijer R, Zwijnenburg D, Diepvens F, Pals G. 2002. Relative quantification of 40 nucleic acid sequences by multiplex ligation-dependent probe amplification. Nucleic Acids Res 30:e57.

Shiloh Y. 2006. The ATM-mediated DNA-damage response: taking shape. Trends Biochem Sci 31:402–410.

Smith PJ, Zhang C, Wang J, Chew SL, Zhang MQ, Krainer AR. 2006. An increased specificity score matrix for the prediction of SF2/ASF-specific exonic splicing enhancers. Hum Mol Genet 15:2490–2508.

Sobeck A. 2001. Caretaker-Gen-Syndrome:Molekulargenetische und Funktionelle Studien. PhD Thesis, Wuerzburg: Julius-Maximilians-University Wuerzburg.

Svedmyr EA, Leibold W, Gatti RA. 1975. Possible use of established cell lines for MLR locus typing. Tissue Antigens 5:186–195.

Telatar M, Teraoka S, Wang Z, Chun HH, Liang T, Castellvi-Bel S, Udar N, Borresen-Dale AL, Chessa L, Bernatowska-Matuszkiewicz E and others. 1998a. Ataxia-telangiectasia: identification and detection of founder-effect mutations in the ATM gene in ethnic populations. Am J Hum Genet 62:86–97.

Telatar M, Wang S, Castellvi-Bel S, Tai LQ, Sheikhavandi S, Regueiro JR, Porras O, Gatti RA. 1998b. A model for ATM heterozygote identification in a large population: four founder-effect ATM mutations identify most of Costa Rican patients with ataxia telangiectasia. Mol Genet Metab 64:36–43.

Teraoka SN, Telatar M, Becker-Catania S, Liang T, Onengut S, Tolun A, Chessa L, Sanal O, Bernatowska E, Gatti RA and others. 1999. Splicing defects in the ataxia-telangiectasia gene, ATM: underlying mutations and consequences. Am J Hum Genet 64:1617–1631.

Udar N, Farzad S, Tai LQ, Bay JO, Gatti RA. 1999. NS22: a highly polymorphic complex microsatellite marker within the ATM gene. Am J Med Genet 82:287–289.

Valentine CR. 1998. The association of nonsense codons with exon skipping. Mutat Res 411:87–117.

Vanagaite L, James MR, Rotman G, Savitsky K, Bar-Shira A, Gilad S, Ziv Y, Uchenik V, Sartiel A, Collins FS and others. 1995. A high-density microsatellite map of the ataxia-telangiectasia locus. Hum Genet 95:451–454.

Westbrook AM, Schiestl RH. 2010. Atm-deficient mice exhibit increased sensitivity to dextran sulfate sodium-induced colitis characterized by elevated DNA damage and persistent immune activation. Cancer Res 70:1875–1884.

Yeo G, Burge CB. 2004. Maximum entropy modeling of short sequence motifs with applications to RNA splicing signals. J Comput Biol 11:377–394.

ELSEVIER

Brain & Development 34 (2012) 287–292

BRAIN & DEVELOPMENT
Official Journal of the Japanese Society of Child Neurology

www.elsevier.com/locate/braindev

Original article

Lesions of cortical GABAergic interneurons and acetylcholine neurons in xeroderma pigmentosum group A

Masaharu Hayashi [a,*], Tatsuyuki Ohto [b], Kei Shioda [c], Ryo Fukatsu [c]

[a] *Department of Brain Development and Neural Regeneration, Tokyo Metropolitan Institute of Medical Science, Tokyo, Japan*
[b] *Department of Pediatrics, Institute of Clinical Medicine, Medical Branch, University of Tsukuba, Ibaraki, Japan*
[c] *Department of Neuropathology, Saitama Medical University, Saitama, Japan*

Received 14 May 2011; received in revised form 28 June 2011; accepted 30 June 2011

Abstract

Xeroderma pigmentosum (XP) is a rare genetic disorder caused by inherited disturbances in the nucleotide excision repair system; patients with XP groups A (XP-A), B, D, and G were shown to have progressive neurological disturbances. Particularly, XP-A patients, which account for approximately half of Japanese XP patients, show severe neurological disorders, including mental retardation and epilepsy. Herein, we performed an immunohistochemical analysis of the number of GABAergic interneurons (GABAis), including calbindin-D28K, parvalbumin, and calretinin, in the cerebral cortex and acetylcholinergic neurons (AchNs) in the nucleus basalis of Meynert (NM) and in the pedunculopontine tegmental nucleus (PPN) in six autopsy cases of XP-A in order to investigate the relationships between mental dysfunction and GABAis and AchNs. The density and percentages of neurons that were immunoreactive for calbindin-D28K and parvalbumin were significantly reduced in the frontal and temporal cortices in XP-A cases, although the density of neurons that were immunoreactive for MAP2 did not differ from that in controls. Additionally, XP-A cases showed reduced AchNs in both the NM and the PPN. The observed reductions of cortical GABAis and AchNs may be involved in the mental disturbances, the higher occurrence of epilepsy, and/or the abnormalities in rapid eye movement sleep in patients with XP-A.

Keywords: Xeroderma pigmentosum; Mental disabilities; Immunohistochemistry; GABA; Acetylcholine; Nucleus basalis of Meynert; Pedunculopontine tegmental nucleus

1. Introduction

Xeroderma pigmentosum (XP) is a rare genetic disorder caused by inherited disturbances in the nucleotide excision repair (NER) system, and complementation studies using cell hybridization have revealed the existence of 8 XP genes (groups A–G and a variant) [1]. Patients with XP groups A, B, D, and G (XP-A, XP-B, XP-D, and XP-G) exhibit progressive neurological disturbances, and XP-A patients, which account for approximately 55% of XP patients in Japan, demonstrate various and severe neurological disorders [2]. Protection from ultraviolet light can prevent the development of skin symptoms but not the neurological disturbances [3]. Although XP-A cases show widespread neuronal loss throughout the central nervous system (CNS) [4], we found a selective impairment of catecholaminergic neurons (CANs) in the basal ganglia and brainstem in autopsy cases, being related to the occurrence of extrapyramidal symptoms and brainstem dysfunction [5].

* Corresponding author. Tel.: +81 3 6834 2334; fax: +81 3 5316 3150.
E-mail address: hayashi-ms@igakuken.or.jp (M. Hayashi).

0387-7604/$ - see front matter © 2011 The Japanese Society of Child Neurology. Published by Elsevier B.V. All rights reserved.
doi:10.1016/j.braindev.2011.06.015

Calcium-binding proteins, such as calbindin-D28K, parvalbumin, and calretinin, regulate intracellular calcium concentrations in neurons and label nonoverlapping populations of GABAergic interneurons (GABAis) in the CNS. In the cerebral cortex, the GABAis are immunoreactive for each calcium-binding protein. We identified selectively disturbed patterns of calcium-binding protein expression in the cerebral cortex in developmental brain disorders [6–8]. However, acetylcholinergic neurons (AchNs) in the nucleus basalis of Meynert (NM) and the pedunculopontine tegmental nucleus (PPN) are involved in mental development and learning abilities [9]. A lesion of the AchN system was observed in developmental brain disorders, such as Down syndrome and Rett syndrome [10,11].

Patients with XP-A suffer from disturbed mental abilities and a worsening of cerebral atrophy according to computed tomography (CT) or magnetic resonance imaging (MRI) studies [3]. Additionally, Japanese XP-A patients showed a higher incidence of epileptic seizures (approximately 15%) than controls [12]. However, the neuropathological background of cortical dysfunction has not been investigated in detail. We performed an immunohistochemical analysis of GABAis in the cerebral cortex and of AchNs in the MyN and PPN in six autopsy cases of XP-A and confirmed that lesions of GABAis and AchNs are involved in the mental abnormalities exhibited by these patients.

2. Materials and methods

2.1. Subjects

Clinical subjects included six cases of clinically and genetically confirmed XP-A and 5 controls with no pathological changes in the central nervous system; subjects were aged from 9 to 47 years (Table 1). Clinical findings in XP-A cases 1–2 and 4–6 were reported previously [4]. The ethical committee of the Tokyo Metropolitan Institute of Medical Science approved this study, and the family of each subject provided informed consent for the postmortem analysis.

2.2. Immunohistochemistry

Brains were fixed in a buffered formalin solution. Each formalin-fixed brain was cut coronally and then embedded in paraffin. Six-μm-thick serial sections were cut from selected brain regions, including the superior frontal cortex, the middle temporal cortex, the hypothalamus including the NM, and the lower midbrain including the PPN. After microwave antigen retrieval, each section was treated with mouse monoclonal antibodies to microtubule-associated protein 2 (MAP2; 1:100, Upstate Cell Signaling Solutions, Billerica, MA, USA), acetylcholinesterase (AchE; Affinity Bioreagents, Inc., Golden, CO, USA), tyrosine hydroxylase (TH; Affinity Bioreagents, Inc.), parvalbumin (PV; Novocastra Laboratories, Newcastle upon Tyne, UK), calbindin-D28K (CD; Novocastra Laboratories), and calretinin (CR; Novocastra Laboratories) at the following concentrations: 1:100 (MAP2, PV, CD, and CR), 1:250 (AchE), and 1:400 (TH). Antibody binding was visualized using the avidin–biotin-immunoperoxidase complex method (Nichirei, Tokyo, Japan) according to the manufacturer's protocol. No staining was detected in the sections in the absence of antibody.

2.3. Quantitative evaluation and data analysis

From the second to the fourth layers in the cerebral cortex, the number of cells immunoreactive for MAP2 and each calcium-binding protein was counted in 6 nonoverlapping microscopic subfields at a 100-fold magnification using a counting box (1 mm^2) to obtain the density of immunoreactive cells. The percentages of cells immunoreactive for each calcium-binding protein relative to those immunoreactive for MAP2 were also

Table 1
Summary of subjects.

	Age (years)	Sex	Cause of death	Post-mortem time (h)	Brain weight (g)
	Controls				
1	9	Male	Acute leukemia	4	n/A
2	16	Male	Pneumonia	6	1505
3	29	Female	Guilain-Barre syndrome	4	n/A
4	36	Female	Thrombotic thromcytopenic purpura	2	1475
5	47	Male	Acute leukemia	10	1400
	Xeroderma pigmentosum group A				
1	19	Male	Candidiasis	2	580
2	19	Male	Renal failure	2	610
3	21	Male	Pneumonia	18	720
4	23	Female	Pneumonia	9	580
5	24	Female	Pneumonia	4	500
6	26	Female	Pneumonia	5	530

Abbreviations: N/A, not accessed.

calculated. In the NM, all AchE-immunoreactive cells were counted ventral to the globus pallidus. The PPN was identified dorsolateral to the rostral superior cerebellar peduncle and the medial lemniscus in the lower midbrain, following the atlas of Olszewski and Baxter [13]. The PPN is composed of clusters of moderately large neurons (pars compacta) and the more widespread pars dissipata in the rostral and medial regions [9]. In the pars compacta of the PPN, the number of cells immunoreactive for MAP2, AchE, TH, and CD were determined after the manual labeling of appropriate cells with nucleoli in 2 serial sections, and the mean value was calculated. The percentages of cells immunoreactive for AchE, TH, and CD relative to those immunoreactive for MAP2 were also calculated. All data are presented as the mean ± SD and analyzed using the nonparametric Mann–Whitney U test in order to compare the results between the XPA cases and controls for a quantitative evaluation of immunoreactive cells. The level of significance was set at $P < 0.05$ to adjust for comparisons.

3. Results

In the cerebral cortex, interneurons immunoreactive for CD, PV, and CR were identified in the second and third layers, near the fourth layer, and from the second to the fourth layers, respectively (Fig. 1A). The density of neurons immunoreactive for MAP2 in the superior frontal cortex and inferior temporal cortex in cases of XP-A did not differ from the average density of that in controls (Table 2). Nevertheless, the density and percentages of neurons immunoreactive for both CD and PV was significantly reduced in the frontal and temporal cortices in cases of XP-A (Fig. 1B). The number and percentage of neurons immunoreactive for CR were reduced in the middle temporal cortex, whereas these values were comparatively preserved in the superior frontal cortex (Table 2). The data suggest a selective impairment of GABAis in the cerebral cortex in cases of XP-A. In the NM, the mean ± SD of the total number of neurons immunoreactive for AchE was 91.7 ± 25.7 in controls (Fig. 1C), and that in XP-A cases was 0.4 ± 0.8, indicating a significant loss of AchNs ($P < 0.01$) (Fig. 1D). In the PPN, the number of neurons immunoreactive for MAP2 in cases of XP-A was reduced to fewer than half of those in controls (Table 3). The numbers and percentages of both AchNs and CANs, which are immunoreactive for AchE and TH (Fig. 1E and F), respectively, were reduced in XP-A cases (Table 3), whereas those immunoreactive for CD remained consistent.

4. Discussion

We previously reported a reduction of CD- and PV-immunoreactive GABAis in the cerebral cortex in samples from patients with various developmental disorders, including neuronal ceroid lipofuscinosis (NCL) [6], dentatorubral–pallidoluysian atrophy (DRPLA) [8], and mucopolysaccharidosis (MPS) [7]. This reduction may be related to the epileptogenesis of progressive myoclonic epilepsy in NCL and DRPLA and the mental disabilities in MPS, respectively. A similar reduction of CD- and PV-immunoreactive GABAis in the cerebral cortex was observed in XP-A cases. XP-A cases exhibited severe brain atrophy (Table 1), and the total number of cerebral neurons was lower than that in controls. However, there was no difference in the density of neurons immunoreactive for MAP2 between controls and XP-A cases (Table 2).

We previously reported that neuronal loss was observed throughout the cerebral cortex in cases of XP-A, and there was no difference in the density of the remaining pyramidal cells between the layers [4]. However, this analysis demonstrated that GABAis are more vulnerable than pyramidal neurons from the second layer to the fourth layers in the cerebral cortex. Evaluating neuronal loss in the brain according to individual subgroups is important for XP-A cases, although the lesion appears to be diffuse and extensive. It is known that GABA receptor-mediated postsynaptic inhibition has important roles in normal cortical function and in controlling events implicated in epileptogenesis, and the decreases in numbers of GABAis and/or postsynaptic inhibition have been reported in the epileptogenic hippocampus and neocortex [14]. The selective loss of CD- and PV-immunoreactive cells was reported in the temporal cortex in Alzheimer's disease and in the prefrontal cortex in schizophrenia [15,16]. The reduction of inhibitory GABAis may be involved in the progressive mental disturbances and the higher occurrence of epilepsyin patients with XP-A. Concurrently, GABAergic anticonvulsants should be used carefully in patients considering the selective reduction of GABAis in the cerebral cortex.

PPN, which is in the lower midbrain, contains cholinergic and noncholinergic neurons and has afferent and efferent connections to the basal ganglia and spinal cord. The cholinergic innervation from the PPN to the thalamus and pons is involved in the generation of muscle tone and rapid eye movement (REM) sleep, and the PPN is believed to be a part of the mesencephalic locomotor region [17]. In controls, there was an age-dependent change in the percentages of AchNs and CANs in the PPN. Cases of perinatal brain damage showed a reduced percentage of AchNs with a compensatory increased percentage of CANs [9]. AchNs were reduced in the PPN in patients with Prader–Willi syndrome, although GABAis in the cerebral cortex, in addition to AchN in the NM, were relatively well-preserved [18].

This analysis revealed a severe reduction in the percentage of AchNs and CANs in the PPN in cases of

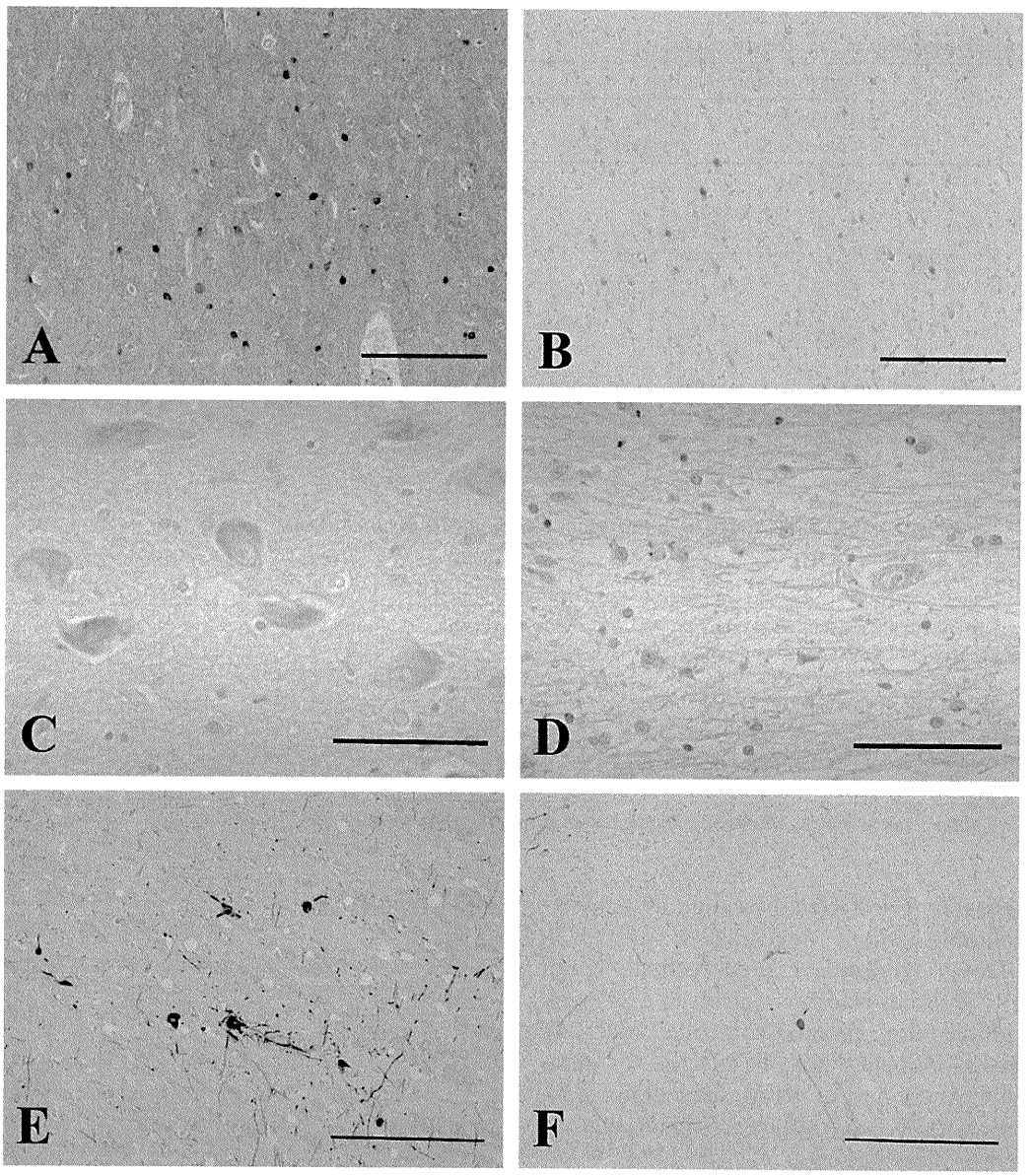

Fig. 1. Representative illustrations of immunohistochemistry in controls and cases of xeroderma pigmentosum group A (XP-A). Immunoreactivities for parvalbumin were found in the interneurons and neuropil around the fourth layer of frontal cortex in control 2 (A), whereas those were reduced in XP-A case 2 (B). Bars = 200 μm. Neurons with cytoplasmic granules immunoreactive for acetylcholine esterase were observed in the nucleus basalis of Meynert in control 3 (C) but not in XP-A case 3 (D). Bars = 100 μm. The pedunculopontine tegmental nucleus had neurons and neuronal processes immunoreactive for tyrosine hydroxylase in control 2 (E), which were reduced in XP-A case 3 (F). Bars = 400 μm.

XP-A, whereas GABAis immunoreactive for CD were relatively spared (Table 3). Unlike the AchNs in Prader-Willi syndrome [18], AchNs were also damaged in the NM. Impairment of CANs seem to occur throughout the CNS, given the reduction of CAN in the basal ganglia and brainstem that we reported previously [5]. Interestingly, a disturbance of motor inhibition during REM sleep was identified in patients with XP-A [19]. Damage of the monoaminergic neurons in the brainstem, including the PPN, may be involved in abnormalities of muscle tone and/or REM sleep, in addition to mental disturbances in patients with XP-A. Recently, we reported successful treatment with low-dose levodopa for laryngeal dystonia, from which many aged patients with XP-A generally suffer [20]. Low-dose levodopa is thought to alleviate dopamine receptor supersensitivity in the basal ganglia. Treatment with donepezil, an acetylcholinergic agent, corrected REM sleep abnormalities in patients with Alzheimer's disease [21] and ameliorated REM sleep behavior disorders in cases of dementia with Lewy bodies [22]. Recently, donepezil has been tested in young adults with Down syndrome [23], in which AchNs were impaired [10,11]. Scores in modified International Classification of